Proc. Natl. Acad. Sci. USA
Vol. 89, pp. 6585–6589, July 1992
Biochemistry

Structure–function relationships of the yeast fatty acid synthase: Negative-stain, cryo-electron microscopy, and image analysis studies of the end views of the structure

(electron microscopy)

JAMES K. STOOPS*, STEVEN J. KOLODZIEJ*, JOHN P. SCHROETER*, JEAN-PIERRE BRETAUDIERE*, AND SALIH J. WAKIL†

*Department of Pathology and Laboratory Medicine, The University of Texas Health Science Center, Houston, TX 77030; and †The Verna and Marrs McLean Department of Biochemistry, Baylor College of Medicine, Houston, TX 77030

Contributed by Salih J. Wakil, March 11, 1992

ABSTRACT **The yeast fatty acid synthase ($M_r = 2.5 \times 10^6$) is organized in an $\alpha_6\beta_6$ complex. In these studies, the synthase structure has been examined by negative-stain and cryo-electron microscopy. Side and end views of the structure indicate that the molecule, shaped similar to a prolate ellipsoid, has a high-density band of protein bisecting its major axis. Stained and frozen-hydrated average images of the end views show an excellent concordance and a hexagonal ring having three each alternating egg- and kidney-shaped features with low-protein-density protrusions extending outward from the egg-shaped features. Images also show that the barrel-like structure is not hollow but has a Y-shaped central core, which appears to make contact with the three egg-shaped features. Numerous side views of the structure give good evidence that the β subunits have an archlike shape. We propose a model for the synthase that has point-group symmetry 32 and six equivalent sites of fatty acid synthesis. The protomeric unit is $\alpha_2\beta_2$. The ends of each of the two archlike β subunits interact with opposite sides of the two dichotomously arranged disclike α subunits. Three such protomeric units form the ring. We propose that the six fatty acid synthesizing centers are composed of two complementary half-α subunits and a β subunit, an arrangement having all the partial activities of the multifunctional enzyme required for fatty acid synthesis.**

The yeast fatty acid synthase ($M_r = 2.5 \times 10^6$) is a multifunctional enzyme composed of two nonidentical subunits, α ($M_r = 207{,}863$) and β ($M_r = 220{,}077$), which are organized in an $\alpha_6\beta_6$ complex (1–3). *A priori*, such a complex might be expected to have six sites of fatty acid synthesis. However, Oesterhelt *et al.* (4) have reported that iodoacetamide, which specifically modifies an active cysteine SH in the β-ketoacyl synthase site, reacts with only three of the six possible sites in the $\alpha_6\beta_6$ complex. As a result of these and genetic studies, it has been proposed that the synthase is half-site active due to negative cooperativity in the action of the condensing enzyme (4–6). However, Stoops and Wakil (7) have found that six cysteine residues are modified by iodoacetamide or 1,3-dibromo-2-propanone in the inactivation of the enzyme, with no evidence of negative cooperativity. In a more convincing study, Singh *et al.* (8) have determined that, on the basis of the stoichiometry of the product synthesized (six moles of fatty acids per mole of enzyme), the enzyme is full-site active. Moreover, kinetic studies of the reaction of *p*-nitrophenyl thioacetate with the enzyme and the determination of the stoichiometry of acetate bound to it have provided further evidence that the enzyme has six equivalent sites of fatty acid synthesis. These studies have shown that the reaction of this ester with the serine residue of the transacetylase site is first order and that, per mole of enzyme, six moles of the acetyl moiety are bound to each of the transacetylase, β-ketoacyl synthase, and 4′-phosphopantetheine domains (9).

Two-dimensional structural studies of the synthase by negative-stain electron microscopy have also been contentious. Wieland *et al.* (10) and Lynen (11) have proposed that the six α subunits form a hexagonal plate to which are attached the six β subunits, three of which extend from each side of the central plate. Stoops *et al.* (1) also have proposed that the six α subunits form a hexagonal plate; however, their study indicated that the attached six β subunits have an archlike shape and are attached to opposite sides of successive α subunits. Numerous efforts to obtain a three-dimensional reconstruction of the molecule from electron microscopy data have yielded a structure with resolution too low to reliably determine the symmetry operator for the structure (12, 13). These efforts have been thwarted by the inability to obtain appropriate alignment of a significant number of the images due to the fact that the major axes of the barrel-like structures are parallel to the support film and, consequently, present a continuum of views (12, 13).

The electron microscopy studies have led to the generally accepted proposal that the center of the barrel-like structure, when viewed down the major axis, would be found to be devoid of protein (hollow barrel), a proposition supported by x-ray scattering studies (14). In the present study, we have obtained a significant number of end views of the structure by utilizing Butvar support film, which makes it possible to obtain multiple views of macromolecules (15). The end view projection of the structure shows protein in its center, thus contradicting the accepted notion that the barrel is hollow. Cryoelectron microscopy studies and the corresponding average image of the end view show a good concordance with the stain results, indicating that the structure has been well preserved by both methods. Consequently, we propose a model which has point group symmetry 32 and six equivalent sites of fatty acid synthesis.

MATERIALS AND METHODS

Enzyme Preparation. Yeast (*Saccharomyces cerevisiae*) fatty acid synthase was prepared and assayed as described previously (9, 16) and had a specific activity of 4000 nmol of NADPH oxidized $min^{-1} \cdot mg^{-1}$. Protein concentrations were determined spectrophotometrically as described previously (1, 17).

Glutaraldehyde Treatment of the Yeast Enzyme. The time course of the reaction of the yeast fatty acid synthase (0.5 mg/ml) with 0.15% glutaraldehyde was monitored by SDS/PAGE. It was determined that over 90% of the α and β

The publication costs of this article were defrayed in part by page charge payment. This article must therefore be hereby marked "*advertisement*" in accordance with 18 U.S.C. §1734 solely to indicate this fact.

subunits were cross-linked by the bifunctional reagent in 2 min in 0.03 M KP_i, pH 7.5/0.1 mM EDTA/1 mM 2-mercaptoethanol at room temperature. Prolonged treatment (>10 min) of the enzyme resulted in considerable aggregation. After 2 min, the protein was diluted 50-fold with 0.25% methylamine tungstate stain and sprayed on Butvar 76-coated copper grids (15).

Electron Microscopy. Yeast fatty acid synthase (11 μg/ml) in 0.25% methylamine tungstate was sprayed on Butvar 76-(Monsanto) or collodion-coated copper grids, as described previously (15). A 3-μl sample containing yeast synthase (0.4 mg/ml), 10 mM sodium phosphate, 1 mM EDTA, and 1 mM cysteine (pH 7.0) was deposited on a glow-discharged, carbon-coated holey grid and prepared for cryoelectron microscopy as described previously (18). Images were recorded on Kodak SO 163 film at ×50,000 by using a JEOL JEM 1200 electron microscope at 100 kV, utilizing conventional irradiation at ≈0.5-μm underfocus and ≈9 e/Å^2 at ≈1.7-μm underfocus for the stain and frozen hydrated specimens, respectively, and developed as described previously (15, 18).

Image Averaging. Image processing was performed on Silicon Graphics (Mountain View, CA) 4D-20 and 4D-25 computers using our SUPRIM image-processing system. Micrographs were digitized up to 4096 × 4096 × 12 bit arrays using an Eikonix 1412 camera adjusted to 5 Å per pixel. Individual particle images were interactively extracted and padded to occupy 64 × 64 arrays. A set of 308 images judged to represent end views of fatty acid synthase were extracted from micrographs of stained material on Butvar film, as were 84 end views of frozen-hydrated particles and 292 end views of stained glutaraldehyde-treated enzyme. Each of the three sets was interactively aligned as described previously (18). After alignment, particles were analyzed by the multivariate statistical technique of correspondence analysis (19) and organized into clusters by hierarchical ascendent classification (20). Cluster averages were generated as previously described (18).

To assess the validity of the threefold symmetry apparent in the average image, the 308 negatively stained end views were realigned to a model produced by sixfold rotational

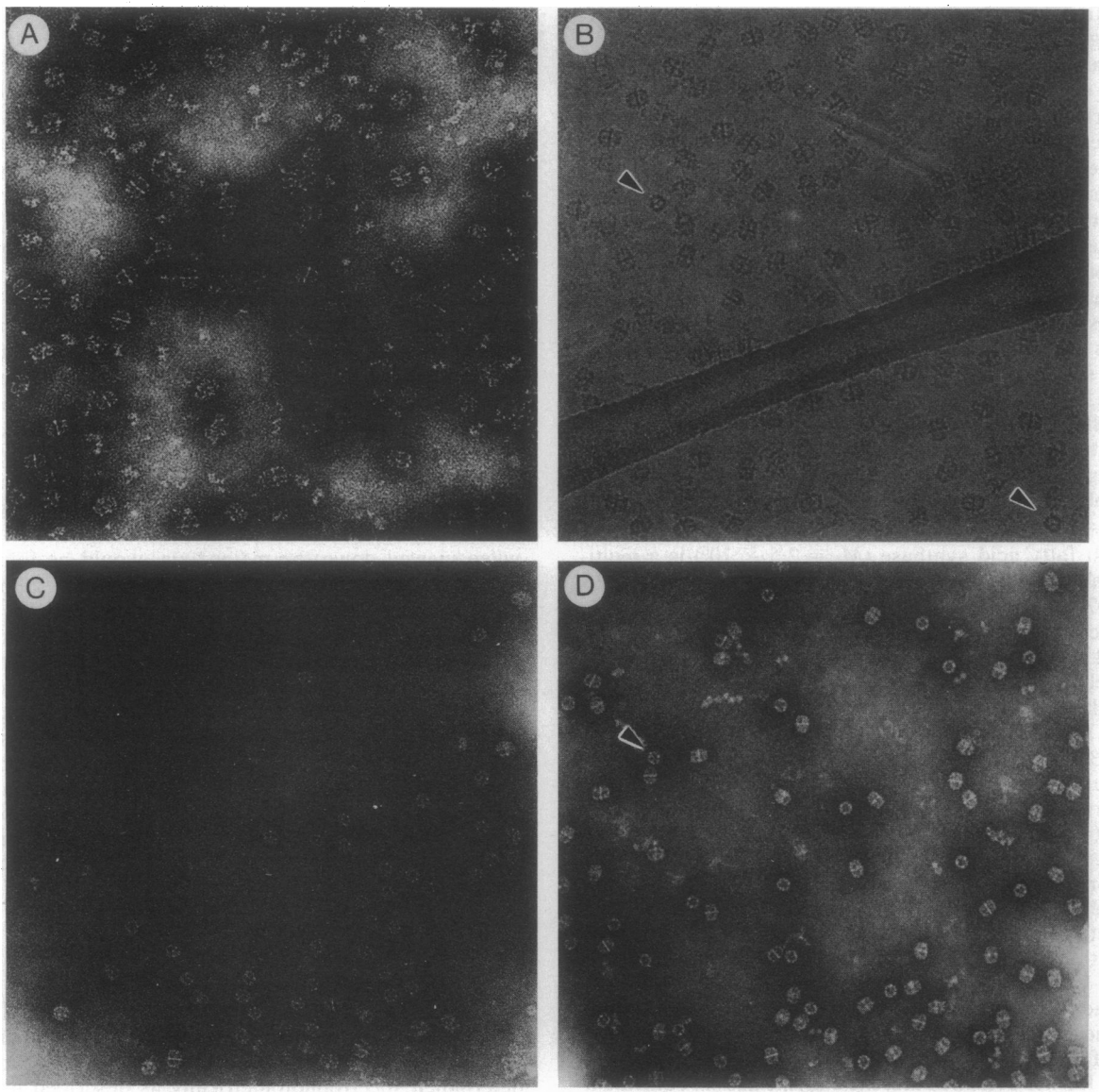

FIG. 1. Electron microscope fields of the yeast fatty acid synthase. (×122,000.) Shown are stained images of the molecules supported on nitrocellulose film (*A*), unstained images in vitreous ice (*B*), stained images on Butvar film (*C*), and stained images of the glutaraldehyde cross-linked enzyme on Butvar film (*D*). In *A* and *B*, the interaction of the molecules with the surfaces results in a predominance of side views of the structure, whereas in *C* and *D* both end views and side views are apparent. The arrows in *B* denote rare end views of the structure in vitreous ice, and the arrow in *D* denotes an end view of the molecule in which the Y-shaped core protein is most apparent.

averaging of this image. Correspondence analysis, followed by hierarchical ascendent classification, was applied to the realigned set, and averages for the first two branches of the tree were produced. The resolution of the average images was estimated from calculations of the spectral signal-to-noise ratios (21). Fine details in the averages were enhanced with a high-pass Butterworth filter (22); the image was then low-pass Fermi filtered (23) at the resolution limit.

RESULTS AND DISCUSSION

Electron Microscopy. In conventional stain electron microscopy, molecules may assume a preferred orientation because they are bound to the support surface (e.g., carbon or nitrocellulose). In the present study, procedures are selected whereby the molecules can assume multiple orientations on the support film. Fig. 1 shows electron microscopic fields of the yeast synthase on nitrocellulose film (*A*), in vitreous ice (*B*), on Butvar film (*C*), and cross-linked with glutaraldehyde on Butvar film (*D*). It is apparent from these fields that the molecule is barrel-shaped with a high-density band of protein that bisects the major axis of the structure. A similar motif obtained by negative-stain electron microscopy has been reported previously (1, 10, 11, 13). Wieland *et al.* (10) have determined by immunoelectron microscopy that the α subunits give rise to the central portion of the molecule, whereas the β subunits extend from it on either side. The fields of the stained and unstained particles (Fig. 1) indicate that the β subunits are archlike, as proposed by Stoops *et al.* (1) and Hackenjos and Schramm (13), rather than being slightly bent rods, as proposed by others (10, 11). To minimize dissociation of the molecule at the low protein concentrations used to prepare the enzyme for microscopy, the synthase was cross-linked with glutaraldehyde. The images obtained (Fig. 1*D*) appear similar to those seen in the other fields (cf. Fig. 1 *A*, *B*, and *C*); however, image analysis showed that considerable loss of some of the structural details has occurred (see below).

On nitrocellulose film and at the air–water interface in vitreous ice, most of the molecules assume an orientation with their major axes parallel to the surfaces (side view), as seen in Fig. 1 *A* and *B*. Two views of structures with their major axes normal to the air–water interface (end views) in vitreous ice are denoted by the arrows in Fig. 1*B*. These views are rare, occurring in a proportion of over 100 side views per end view. It was determined that the preferred orientation is independent of the thickness of the ice (data not shown), ruling out the possibility that ice depth limits the number of end views of the structure. Instead, apparently surface interactions induce a preferential orientation of the molecules, and some proteins appear to have strong interactions at the air–water interface in specimens prepared for cryo-electron microscopy (24). Further, this and previous studies (1, 10, 11, 13) suggest that interaction of the yeast synthase with the support films also results in mainly side views of the structure. Nevertheless, even though the enzyme interacts with the surfaces, the variant images seen in Fig. 1 *A* and *B* indicate that the molecule is free to rotate about its major axis. Some of the side views indicate that the molecules may have a twofold axis of symmetry, but the inability to obtain side views of the structure with a preferred orientation has made it difficult to align these images.

Macromolecules interact little or not at all with the Butvar support film (15), thus making it possible to obtain multiple views of their structures (15, 18, 25, 26). This film has been exploited in the present study to obtain side and end views of the structure (Fig. 1 *C* and *D*). Experiments in which the stage was rotated 50° indicate the ring and oval shapes are orthogonal views of the structure (data not shown). The end views of the molecule reveal a threefold axis of symmetry and show that the barrel-like structure is not hollow but, instead, has protein located on this axis in the projected shape of a Y (Fig. 1*D*, image denoted by the arrow). The two end views of the structure in vitreous ice (Fig. 1*B*) corroborate the stain findings, and the average image (derived from 84 end views obtained in ice) shows that the Y-shaped central core is not an artifact of the stain (see below).

Like the side views, the end views of the particles in stain and vitreous ice show that the molecules are free to rotate about their major axes. However, the prominent features associated with these end views, and the fact that they correspond to multiple views of the same projection of the structure, have made it possible to align a large number of the particles and perform image analysis.

Image Averaging. The average image of the end views of the structure generated from stain and cryo-electron microscopy shows that the protein in the outer ring is distributed in a hexagonal configuration (Fig. 2) and that the structural features have a threefold axis of symmetry. The ring is composed of three each alternating egg- and kidney-shaped

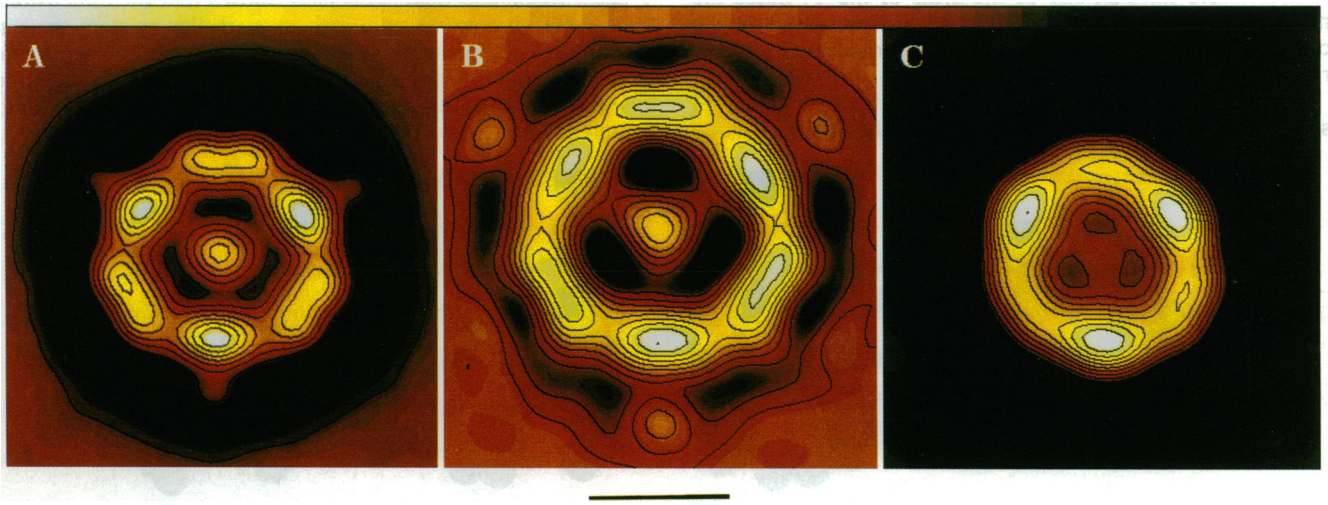

FIG. 2. Average images of 308, 84, and 292 end views of the structure derived from the stained (*A*), frozen-hydrated (*B*), and glutaraldehyde cross-linked stained (*C*) data. The resolution of these images is 30.6 ± 1.9, 40.5 ± 4.0, and 33.1 ± 2.7 Å, respectively. The scale bar corresponds to 100 Å and the color bar denotes relative protein density from high (white) to low (dark). The stained images are approximately 20% smaller than the frozen-hydrated image.

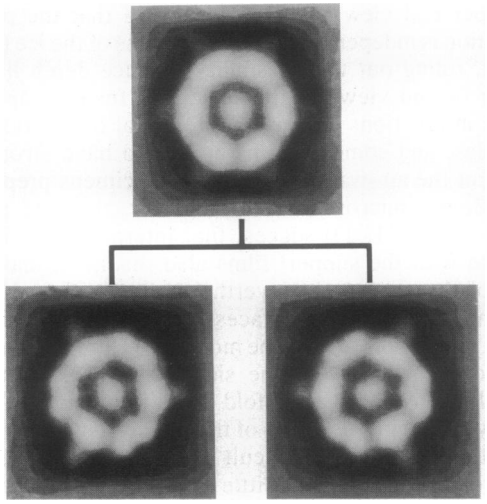

FIG. 3. Correspondence analysis followed by hierarchical ascendent classification of the stained images aligned to an artificially generated model with sixfold symmetry. The upper image is the grand average of 308 images showing the expected sixfold symmetry. The two lower images are averages of the two major clusters (n = 153 and n = 155). These images are threefold symmetric but rotated by 60° with respect to one another. The sixfold grand average is thus seen to arise from two misaligned threefold symmetric subimages.

objects (Fig. 2 *A* and *B*). In the average image, the egg-like shapes appear to have higher protein density than do the kidney-like shapes. The protein in the center of the average image is arranged in a Y shape such that the three arms of the Y are directed toward and appear to make contact with the three egg-shaped objects in the outer ring. In addition, each egg-shaped object has a low-protein-density protrusion that extends outward from the ring.

Correspondence analysis of the stain data shown in Fig. 2*A*, followed by hierarchical ascendent classification, showed that the data set divided into five major clusters of average images having minor differences both in the density distribution around the ring and in the central region. However, all five cluster averages exhibited threefold symmetry and showed the outer ring projections spaced symmetrically around the ring. Although some of the clusters lost the threefold symmetry of the central region, there was no evidence of a subcluster with a sixfold center. Rather, these clusters were missing one of the arms of the Y. Since the major features of the grand average are preserved in the cluster averages, we conclude that the grand average correctly represents the data sets.

To assure that model choice of molecules with threefold symmetry did not dictate the symmetry of the final image, the average image for the stain data (Fig. 2*A*) was rotationally averaged to exhibit sixfold symmetry and used as the starting model in a separate alignment. The average image for this alignment exhibited the expected sixfold symmetry (Fig. 3). The data derived from correspondence analysis of this aligned set of images, followed by hierarchical ascendent classification, indicated two major clusters of approximately equal size that were threefold symmetric and rotated 60° with respect to each other (Fig. 3). A similar result was obtained from the glutaraldehyde data set (data not shown). Further, the possibility that the threefold symmetry results from a different environment of the β subunits in the stain (e.g., three β subunits directed toward the support film and three away from it) is unlikely, since the threefold symmetry is also associated with the frozen-hydrated image (Fig. 2*B*). These results constitute strong evidence that the threefold symmetry apparent in the average images shown in Fig. 2 is not a consequence of the models chosen in the initial alignment or of the support film. The threefold symmetry revealed by the average image of the end views of the structures negates, then, the models proposed earlier (1, 10, 11), which would exhibit sixfold symmetry when viewed from this perspective.

Table 1. Dimensions from the images of the yeast fatty acid synthase

Image	Dimension, Å: Diameter of outer/inner ring*	Dimension, Å: Length of major axis†	Dimension, Å: Center of mass to center of mass‡	Percent difference from frozen-hydrated§
Frozen-hydrated	218/104	247	162	—
Stained	186/84	213	133	−18
Glutaraldehyde stained	180/76	193	123	−24

*Estimated from the average images (end view).
†Estimated from the length of the images in the microscope fields (side view).
‡Distance between the center of the egg- and kidney-shaped features diagonally opposite each other in the ring. These values give the best estimate of the difference in the size of the images.
§Based on the values estimated in ‡.

Table 1 shows the dimensions for the average images compared with their corresponding features for the stained and frozen-hydrated specimens. The dimensions derived from the stain data set are approximately 20% less than the corresponding values derived from the frozen-hydrated images. Olson and Baker (27) have shown that the dimensions of some virus particles are 6–30% smaller in stain than in vitreous ice, presumably resulting from shrinkage in the stain. If this is so, the yeast synthase may have undergone some shrinkage during its preparation in methylamine tungstate stain.

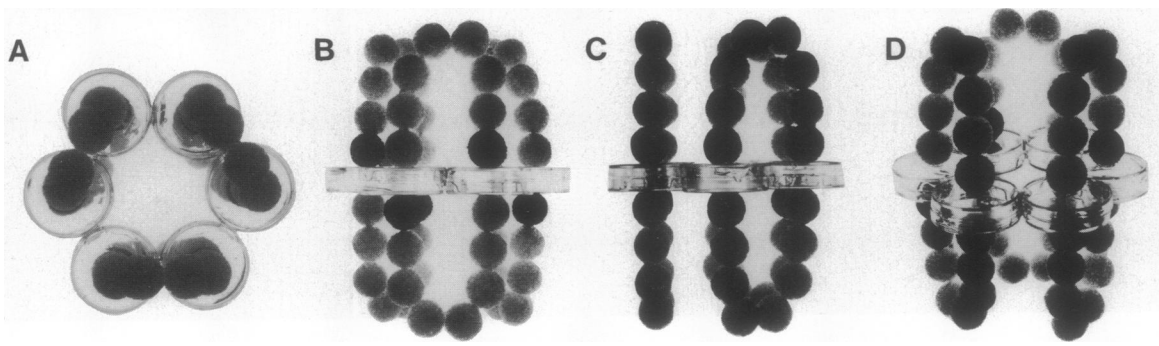

FIG. 4. Three unique views of the proposed model for the yeast fatty acid synthase. Orthogonal views, end (*A*) and side (*B* and *C*), exhibit threefold and twofold axes of symmetry, respectively. *B* and *C* are related by a 30° rotation of the structure about its major axis. In *D*, the side view is slightly tilted to show the relationship between the arches and the hexagonal ring. The protein in the center of the molecule has been omitted in the model (see text). The other images seen in the electron microscopy fields appear to be intermediate between these three views.

The important finding is that, regardless of any shrinkage the structure has undergone in stain, the good concordance of the features obtained by stain and cryoelectron microscopy indicates that the structural design has been well preserved by both methods. Further, these studies show that, in contrast, even limited treatment of a molecule with glutaraldehyde, a reagent employed to stabilize oligomeric proteins (often after extensive exposure to glutaraldehyde) for electron microscopy studies, can result in significant perturbations to its structure (Fig. 2*C*): the alternating kidney-shaped objects and the protein extensions from the egg-shaped objects were lost.

Model. The structural model of the yeast synthase shown in Fig. 4 has three unique projections. Inspection of many fields of the molecules reveals images that are similar or intermediate to these views. In this model, the protein in the center of the structure has been omitted, since we have no information regarding its location on the threefold axis. The model has point-group symmetry 32 with three protomeric units of $\alpha_2\beta_2$ that make up the ring, similar to a hypothetical arrangement that has been previously proposed (13). We propose that the two superimposed β subunits and the underlying two α subunits give rise to an egg-shaped image, one that exhibits higher protein density in the end view of the structure (Fig. 2). The kidney-shaped object, with its lower protein density, may represent the three connections between adjacent α subunits outside of the arches (Fig. 4). This model has two sets of three interacting sites located between adjacent α subunits arranged head-to-tail in a hexagonal ring. Thus, the α subunits are related to each other by a 180° rotation about an axis normal to the ring. It is further proposed that two half-α subunits under the arch and the β subunit make up a center for fatty acid synthesis. It is apparent that this arrangement can give rise to six equivalent reaction centers, which is consistent with the functional studies (8, 9) that indicate the enzyme has full-site activity.

The end views of the yeast synthase structure have given new insight into its structural organization. It is clear that the structure depicted in the model shown in Fig. 4 is more complex than previously proposed (1, 10, 11, 13). Besides the Y-shaped configuration of protein that lies on the major axis of the structure, significant protein density protrudes outward from the central ring on the threefold axis of symmetry. The origin and function of these features cannot be deduced from the present studies. In addition, our present model oversimplifies the shape of the α and β subunits since it does not accommodate the alternating egg- and kidney-shaped features seen in the average images of the end views of the structure (Fig. 2; cf. Fig. 4).

To gain further insight into the structural organization of the complex, a three-dimensional reconstruction of the molecule is needed. In this regard, two previous three-dimensional reconstructions from a single image and from eight images lacked statistical significance and their low resolution gave little insight into the structural organization of the complex (12, 13). The present studies provide substantial indication that a meaningful reconstruction can be performed utilizing the numerous and readily alignable end views of the molecule that are afforded by the Butvar support film.

J.K.S. is grateful to Norman Olson and Timothy Baker at Purdue University for instructions in the techniques associated with cryoelectron microscopy and B. V. V. Prasad at Baylor College of Medicine for instruction on the use of the electron microscope for this purpose. We thank B. Lee Ligon for editorial assistance. This study was supported in part by Grants GM-46278, HL-42886, and GM-39536 from the U.S. Public Health Service to J.K.S. and Grant GM-19091 from the U.S. Public Health Service, Grant Q-587 from the Robert A. Welch Foundation, and a grant from The Clayton Foundation for Research to S.J.W. A preliminary report of this study was presented at the annual meeting of the Federation of American Societies for Experimental Biology, New Orleans, LA, June 4–7, 1990 (28).

1. Stoops, J. K., Awad, E. S., Arslanian, M. J., Gunsberg, S., Wakil, S. J. & Oliver, R. M. (1978) *J. Biol. Chem.* **253,** 4464–4475.
2. Chirala, S. S., Kuziora, M. A., Spector, D. M. & Wakil, S. J. (1987) *J. Biol. Chem.* **262,** 4231–4240.
3. Mohamed, A. H., Chirala, S. S., Mody, N. H., Huang, W.-Y. & Wakil, S. J. (1988) *J. Biol. Chem.* **263,** 12315–12325.
4. Oesterhelt, D., Bauer, H., Kresze, G.-B., Steber, L. & Lynen, F. (1977) *Eur. J. Biochem.* **79,** 173–180.
5. Schweizer, E. (1984) in *Fatty Acid Metabolism and Its Regulation*, ed. Numa, S. (Elsevier, Amsterdam), pp. 59–83.
6. Schweizer, M. (1986) in *Multidomain Proteins*, eds. Hardie, D. G. & Coggins, J. R. (Elsevier, Amsterdam), pp. 195–227.
7. Stoops, J. K. & Wakil, S. J. (1981) *J. Biol. Chem.* **256,** 8364–8370.
8. Singh, N., Wakil, S. J. & Stoops, J. K. (1985) *Biochemistry* **24,** 6598–6602.
9. Stoops, J. K., Singh, N. & Wakil, S. J. (1990) *J. Biol. Chem.* **265,** 16971–16977.
10. Wieland, F., Siess, E. A., Renner, L., Verfurth, C. & Lynen, F. (1978) *Proc. Natl. Acad. Sci. USA* **75,** 5792–5796.
11. Lynen, F. (1980) *Eur. J. Biochem.* **112,** 431–442.
12. Hoppe, W., Schramm, H. J., Sturm, M., Hunsmann, N. & Gassmann, J. (1976) *Z. Naturforsch. A* **31,** 1380–1390.
13. Hackenjos, W.-A. & Schramm, H. J. (1987) *Biol. Chem. Hoppe-Seyler* **368,** 19–36.
14. Pilz, I., Herbst, M., Kratky, O., Oesterhelt, D. & Lynen, F. (1970) *Eur. J. Biochem.* **13,** 55–64.
15. Stoops, J. K., Momany, C., Ernst, S. R., Oliver, R. M., Schroeter, J. P., Bretaudiere, J.-P. & Hackert, M. L. (1991) *J. Electron Microsc. Tech.* **18,** 157–166.
16. Stoops, J. K., Arslanian, M., Oh, Y. H., Aune, K. C., Vanaman, T. C. & Wakil, S. J. (1975) *Proc. Natl. Acad. Sci. USA* **72,** 1940–1944.
17. Stoops, J. K., Arslanian, M. J., Aune, K. C. & Wakil, S. J. (1978) *Arch. Biochem. Biophys.* **188,** 348–359.
18. Stoops, J. K., Schroeter, J. P., Bretaudiere, J.-P., Olson, N. H., Baker, T. S. & Strickland, D. K. (1991) *J. Struct. Biol.* **106,** 172–178.
19. Van Heel, M. & Frank, J. (1981) *Ultramicroscopy* **6,** 187–194.
20. Benzecri, J.-P. (1982) *Les Cahiers de l'Analyse des Donne'es* **7,** 209–218.
21. Unser, M., Trus, B. L. & Steven, A. C. (1987) *Ultramicroscopy* **23,** 39–52.
22. Gonzalez, R. C. & Wintz, P. (1987) *Digital Image Processing* (Addison-Wesley, London), 2nd Ed., pp. 170–171.
23. Frank, J., Verschoor, A. & Wagenknecht, T. (1985) in *New Methodologies in Studies of Protein Conformation*, ed. Wu, T. T. (Van Norstrand-Rhinehold, New York), pp. 36–89.
24. Dubochet, J., Adrian, M., Chang, M.-J., Homo, J.-C., Lepault, J., McDowell, A. W. & Schultz, P. (1988) *Q. Rev. Biophys.* **21,** 29–228.
25. Stoops, J. K., Bretaudiere, J.-P. & Strickland, D. K. (1989) *Biochem. Biophys. Res. Commun.* **161,** 216–220.
26. Bretaudiere, J.-P., Bretaudiere, J. T. & Stoops, J. K. (1988) *Proc. Natl. Acad. Sci. USA* **85,** 1437–1441.
27. Olson, N. H. & Baker, T. S. (1989) *Ultramicroscopy* **30,** 281–298.
28. Bretaudiere, J.-P., Mohamed, A. H., Wakil, S. J. & Stoops, J. K. (1990) *FASEB J.* **4,** 2135 (abstr.).